

# The Physical Conditions and Dynamics of the Interstellar Medium in the Nucleus of M83: Observations of CO and C I

Glen R. Petitpas and Christine D. Wilson

McMaster University, 1280 Main Street West, Hamilton Ontario, Canada L8S 4M1

## ABSTRACT

This paper presents [C I],  $^{12}\text{CO } J=4-3$ , and  $^{12}\text{CO } J=3-2$  maps of the barred spiral galaxy M83 taken at the James Clerk Maxwell Telescope. Observations indicate a double peaked structure which is consistent with gas inflow along the bar collecting at the inner Lindblad resonance. This structure suggests that nuclear starbursts can occur even in galaxies where this inflow/collection occurs, in contrast to previous studies of barred spiral galaxies. However, the observations also suggest that the double peaked emission may be the result of a rotating molecular ring oriented nearly perpendicular to the main disk of the galaxy. The  $^{12}\text{CO } J=4-3$  data indicate the presence of warm gas in the nucleus that is not apparent in the lower  $J$  CO observations, which suggests that  $^{12}\text{CO } J=1-0$  emission may not be a reliable tracer of molecular gas in starburst galaxies. The twelve [C I]/ $^{12}\text{CO } J=4-3$  line ratios in the inner  $24'' \times 24''$  are uniform at the  $2\sigma$  level, which indicates that the  $^{12}\text{CO } J=4-3$  emission is originating in the same hot photon-dominated regions as the [C I] emission. The  $^{12}\text{CO } J=4-3/J=3-2$  line ratios vary significantly within the nucleus with the higher line ratios occurring away from peaks of emission along an arc of active star forming regions. These high line ratios ( $>1$ ) likely indicate optically thin gas created by the high temperatures caused by star forming regions in the nucleus of this starburst galaxy.

*Subject headings:* galaxies: barred spiral — galaxies: individual (M83) — galaxies: ISM — galaxies: starburst — ISM: molecules

## 1. Introduction

The circumnuclear regions of galaxies are very often the setting for starbursts and other extraordinary events. Observations of the gas kinematics and distribution indicate that bars, resonances, gas inflow, and tidal shear play important roles in the formation and evolution of nuclear starbursts (e.g. Handa et al. 1990; Kenney et al. 1992). Previous observations show that the molecular gas in the central regions of barred spiral galaxies often does not extend all the way into the centre of the nucleus. It accumulates some distance away from the centre, giving the emission a double peaked appearance with each peak occurring where the bar meets the nucleus (Kenney et al. 1992; Ishizuki et al. 1990). Dynamical models indicate that in the presence of a

barred potential, gas will flow inward along the bar and slow its descent temporarily near inner Lindblad resonances (ILR, e.g. Combes 1988; Shlosman, Frank & Begelman 1989). At these locations the gas may accumulate into larger complexes of molecular clouds.

In addition to complex dynamics, there is most likely a profusion of complicated photo-chemistry occurring within the nuclei of starburst galaxies. Interstellar clouds are believed to consist of smaller high density dark cores interspersed throughout a larger region of lower density. These high density regions are self-shielded from ultraviolet (UV) radiation that tends to dissociate molecular gas. The result is the population of the diffuse region by hydrogen atoms (H I), atomic and ionized carbon (C, C<sup>+</sup>), and many other atomic and ionized species (e.g. Morton et al. 1973), while the dark cores can contain molecular species such as H<sub>2</sub> and CO.

It is believed that atomic carbon can exist only in a small energy window, outside of which it will either be ionized or combined with oxygen to form CO. Inside the dense cores, most of the carbon combines to form CO, while outside the cores, the UV radiation acts to ionize atomic carbon. It is therefore expected that C I is the dominant species near the edges of dense, self-shielding cloud cores.

This simple model fails to explain the extended [C I] emission observed in molecular clouds in our own Galaxy (Plume, Jaffe, & Keene 1994; Keene et al. 1985). One possible explanation is found in the clumpy structure of molecular clouds (e.g. Stutzki & Güsten 1990). This clumpiness would allow UV radiation to penetrate much deeper into the cloud allowing atomic carbon to exist at depths greater than would be allowed by a simple spherical model of molecular clouds (e.g. Boisse 1990). Many alternative explanations have been proposed to explain the extended [C I] emission. These ideas range from complicated chemical processes involving H<sup>+</sup> (Leung, Herbst, & Heubner 1984) to simpler ideas such as a C/O ratio greater than one (e.g. Keene et al. 1985).

This paper presents [C I] and CO maps of the barred spiral galaxy M83. Its low inclination angle ( $i = 24^\circ$ , Comte 1981) and close proximity ( $D = 4.7$  Mpc, Tully 1988) make it one of the best locations for studying the response of gas to a barred potential. It is believed to be undergoing a nuclear starburst (e.g. Talbot et al. 1979), which may have been triggered by molecular gas inflow along the bar potential. This nuclear starburst would produce higher temperatures which should readily excite the higher  $J$ -transitions in the CO gas. Also, strong UV flux has been detected in the nucleus (Bohlin et al. 1983), which would help dissociate the CO into atomic carbon. By studying the CO and [C I] data, we can understand better the dynamics of the gas and its role in fueling the nuclear starburst and also learn about the conditions conducive to the formation of atomic carbon.

## 2. Observations and Data Reduction

[C I], <sup>12</sup>CO  $J=4-3$ , and <sup>12</sup>CO  $J=3-2$  observations of M83 were taken using the 15 m James Clerk Maxwell Telescope (JCMT) over the period of 1996 April 5 – 10. The half-power beam

width of the JCMT is  $12''$  at 492 GHz ([C I]) and 461 GHz ( $^{12}\text{CO } J=4-3$ ) and  $14''$  at 345 GHz ( $^{12}\text{CO } J=3-2$ ). The galaxy was mapped using  $5''$  sampling in all transitions. All observations were obtained using the Dwingeloo Autocorrelation Spectrometer.

The data were reduced using the data reduction package SPECX and were binned to  $4 \text{ km s}^{-1}$  resolution. The raw spectra were converted into FITS files using SPECX and then the Bell Labs data reduction package COMB was used to convolve the  $^{12}\text{CO } J=4-3$  to the same beam size as the  $^{12}\text{CO } J=3-2$  data. The  $^{12}\text{CO } J=3-2$  data were taken in raster mode at the JCMT. It was later discovered that a loose wire was causing poor baselines for spectra taken in this manner so the  $^{12}\text{CO } J=4-3$  and [C I] data were taken in beam-switched mode. The beam was switched to a position  $60''$  perpendicular to the bar, which we assume to have negligible emission with respect to the on-positions located along the galactic bar. The data were binned and zeroth order baselines were removed. The poorer baselines encountered for the  $^{12}\text{CO } J=3-2$  raster maps resulted in poor cosmetic appearance of the intensity maps in the regions without emission, but did not noticeably effect the line parameters. Pointing was checked frequently and was typically less than  $2''$  rms. The calibration was monitored by frequently observing both planets and spectral line calibrators. The spectral line calibrators for the CO data had integrated intensities that were within  $\sim 10\%$  of the published values. We therefore adopt the values of  $\eta_{\text{MB}} = 0.58$  for  $^{12}\text{CO } J=3-2$  and  $\eta_{\text{MB}} = 0.52$  for the  $^{12}\text{CO } J=4-3$  and [C I] data as given in the JCMT User’s Guide.

Since the line strengths we are comparing are measured with (or convolved to) the same beam diameter, using the  $T_{\text{R}}^*$  temperature scale would ensure that our observed line ratios are equal to the true radiation temperature ratios. However, conversion to  $T_{\text{R}}^*$  from  $T_{\text{A}}^*$  requires knowledge of the forward scattering and spillover ( $\eta_{\text{FSS}}$ ), which is difficult to measure and was not attempted during the observing run. We do have good values for the main beam efficiencies and so an accurate conversion to main beam temperature ( $T_{\text{MB}}$ ) is possible. Using the  $T_{\text{MB}}$  scale instead of  $T_{\text{R}}^*$  scale only changes the  $^{12}\text{CO } J=4-3/J=3-2$  line ratio by  $\sim 10\%$  under normal calibration conditions. For this reason, we will use the main beam temperature scale for the line ratios throughout this paper. The maps are also plotted in the  $T_{\text{MB}}$  temperature scale. The individual  $^{12}\text{CO } J=3-2$ ,  $^{12}\text{CO } J=4-3$ , and [C I] spectra are shown in Figures 1, 2, and 3 respectively.

### 3. Morphology and Dynamics

The integrated intensity maps in the three lines (Figures 4–6) indicate a double (possibly triple) peaked structure in the emission. Within the pointing uncertainty of the JCMT ( $2''$  rms), each map exhibits the strongest emission peak at  $(+5'', +5'')$  with the second strongest at  $(-5'', -10'')$ . These two emitting regions peak at different velocities: the channel maps (Figures 7–8) show that the emission at  $(+5'', +5'')$  peaks at approximately  $500 \text{ km s}^{-1}$  in both the  $^{12}\text{CO } J=3-2$  and  $^{12}\text{CO } J=4-3$  maps, while the emission at  $(-5'', -10'')$  peaks at  $\sim 550 \text{ km s}^{-1}$ . The [C I] emission is too weak to obtain reliable channel maps. In the integrated intensity maps (especially [C I] and  $^{12}\text{CO } J=4-3$ ), there are indications of a third, weaker peak at approximately

( $-10''$ ,  $-5''$ ), but the channel maps do not indicate a separate clump of emission at a velocity different from the two main emission peaks. The channel maps suggest that the hints of a third emission peak are likely just an extension of the ( $-5''$ ,  $-10''$ ) peak.

### 3.1. Gas Collection at Lindblad Resonances?

Figures 4, 5, and 6 clearly show that the [C I] emission appears to follow the  $^{12}\text{CO } J=4-3$  emission much more closely than it does the  $^{12}\text{CO } J=3-2$  emission. The  $^{12}\text{CO } J=4-3$  and [C I] emission appear asymmetric, with the two main peaks to the north and south of the centre connected by an “elbow” of weaker emission that undergoes a bend of  $\sim 90^\circ$ . Irregular structure was also seen in M83 in the  $^{12}\text{CO } J=1-0$  emission by Handa et al. (1990). Numerical simulations predict that a shock front will form at the leading edge of the bar (e.g. Sørensen et al. 1976). At this shock front, interstellar gas is compressed and loses kinetic energy, which causes it to flow toward the nucleus. The star formation along the bar is thought to be triggered by such an inflow. In the figures, where the galactic bar of M83 runs along the  $x$ -axis, it is clear that the emission is originating on the leading edge of the bar potential as predicted by theoretical models of barred galaxies. This geometry in M83 was first identified by Handa et al. (1990).

One important question is why the gas does not continue to flow into the centre of the galaxy. It has been suggested (e.g. Kenney et al. 1992) that the location of the ILR is often coincident with the double peaks of molecular gas often seen in barred spiral galaxies. They studied several barred spiral galaxies and found that galaxies without nuclear starbursts exhibit a double peaked emission structure, while the galaxy with the nuclear starburst has a single peak of emission at the center. This result suggests that accumulation of gas at ILRs is a way of inhibiting nuclear starbursts in barred spiral galaxies. Moreover, as calculations indicate the starburst galaxy does contain ILRs, the mere existence of ILRs does not appear to be sufficient to prevent starbursts (Kenney et al. 1992).

Although we cannot directly calculate the locations of the ILRs from our data or existing data (although see Gallais et al. (1994) for a good attempt), the double peaked structure we see in M83 is very similar to that observed in the non-starburst galaxies of Kenney et al. (1992) and most likely indicates gas collection at an ILR. We also note that M83 is undergoing a nuclear starburst (e.g. Talbot et al. 1979) which suggests that *a nuclear starburst may occur even in galaxies that exhibit this double peaked structure*, in contrast to the findings of Kenney et al. (1992). A better rotation curve for the nucleus of M83 will provide the true location on the ILRs, thus proving or disproving the above result.

High resolution  $^{12}\text{CO } J=1-0$  maps by Handa, Ishizuki, & Kawabe (1994) show that the double peaked structure of M83 straddles a nuclear star formation complex traced by radio continuum emission (Cowen & Branch 1985). They do not see strong  $^{12}\text{CO } J=1-0$  emission from within the central star forming region itself. Our  $^{12}\text{CO } J=3-2$  data show a very similar structure

(Figure 7,  $V_{\text{LSR}} = 520 \text{ km s}^{-1}$ ). Moreover, the  $^{12}\text{CO } J=4-3$  data (Figure 8) show a very different structure; at  $520 \text{ km s}^{-1}$ , the  $^{12}\text{CO } J=4-3$  emission *peaks* at the centre of the star forming region. These data suggest that there *is* molecular gas in the nuclear regions of M83, but it is heated by the nuclear starburst so that most of the CO is collisionally excited to the higher rotational ( $J$ ) states. This result, combined with the double peaked accumulations of  $^{12}\text{CO } J=4-3$  emission seen in the integrated intensity maps (Figure 5), suggests that molecular gas gathers at the ILR before eventually flowing into the nucleus where the starburst occurs. The gas at the ILRs would be heated less intensely by the starburst than the gas in the nucleus, so in the double peaks we see emission from cooler gas (as traced by  $^{12}\text{CO } J=1-0$  emission) as well as hotter gas (as traced by  $^{12}\text{CO } J=3-2$  and  $^{12}\text{CO } J=4-3$  emission), while in the nucleus most of the gas is in the  $J = 4$  and higher states. This result indicates that  $^{12}\text{CO } J=1-0$  emission is not always a good tracer of the molecular gas in starburst galaxies, as is often assumed. The edge-on starburst galaxy M82 exhibits a similar structure with the  $^{12}\text{CO } J=4-3$  data filling in the torus of rotating gas traced by the  $^{12}\text{CO } J=3-2$  emission (White et al. 1994; Tilanus et al. 1991).

### 3.2. Rotating Gas Disk/Torus Out of the Plane of the Galaxy?

An alternate explanation for the observed CO morphology and kinematics in M83 is the existence of a rotating torus of molecular gas (cf. M82, Tilanus et al. 1991, NGC 253, Israel et al. 1995; both also starburst galaxies). However, the observed  $^{12}\text{CO } J=4-3$  emission that peaks at the centre of the nucleus is not consistent with a simple torus model. Nevertheless, the nuclear  $^{12}\text{CO } J=4-3$  emission could be explained if the CO gas is actually a disk/torus combination. The nuclear  $^{12}\text{CO } J=4-3$  emission could originate in a disk of hotter molecular gas located inside a molecular torus of gas. In this picture, the torus would consist of slightly cooler gas that allows for the presence of the lower  $J$  states.

It has been proposed (e.g. Larkin et al. 1994) that a torus of gas may accumulate in the regions between the inner and outer ILRs. While this may be occurring in M83, the problem is that the morphology requires the torus/disk to be seen nearly edge-on. Since M83 has an inclination angle of only  $24^\circ$ , only a torus lying out of the plane of the galaxy could possibly produce the observed morphology. However, it is not entirely unreasonable that there could be a torus/disk of gas that lies out of the plane of the galaxy. Kinematically distinct subsystems have been found in at least three disk galaxies (NGC 3672, NGC 4826, and NGC 253, see Anantharamaiah & Goss 1996). This configuration may be more common than the observations indicate due to a selection effect caused by the high levels of extinction in the nuclear regions of disk galaxies. M83 has long been believed to have a disk that is quite warped (Rogstad, Lockhart, & Wright 1974), while more recent observations of dust lanes suggest that M83 is undergoing three-dimensional accretion in the nucleus and that the nuclear dust lanes pass out of the plane of the galaxy (Sofue & Wakamatsu 1994). This model would be generally consistent with the idea of a tilted torus of molecular gas. Dust tends to trace regions of high density, while molecules need higher densities

to be shielded from dissociation by UV flux. Hence, it is reasonable to expect a ring of molecular gas to be coincident with the ring formed by the warped dust lanes that lie out of the plane of the galaxy.

One problem with the above discussion is explaining *how* the inner part of the disk of M83 could become misaligned with the rest of the disk of the galaxy. One possible explanation is that M83 has accreted a smaller companion galaxy. Simulations of disk galaxies accreting a smaller companion have shown that these ‘minor mergers’ are able to produce warped disks, large spiral arms, and radial inflow of gas that may trigger nuclear starbursts (e.g. Quinn et al. 1993; Mihos & Hernquist 1994; Hernquist & Mihos 1995). If the companion was small enough, it may remain intact as it settles into the nucleus of the larger galaxy (e.g. Balcells & Quinn 1990). The rotation curve that would be created by the combination of the two rotating objects would appear very peculiar. It may manifest itself as a discontinuity at the radius of the smaller galaxy that has been accreted to the core of the larger galaxy. Such a rotation curve has been predicted by the model of Handa et al. (1990) who fitted the *outer* rotation curve of M83 in an attempt to determine the rotation curve of the inner regions. If an accretion event is the cause of the proposed inner disk misalignment, it is not clear whether such a system would have Lindblad resonances where gas could collect. Better models of mergers of barred galaxies as well as observation of the inner rotation curve for M83 will yield a clearer picture of the dynamics at work.

## 4. Physical Conditions

Determining the physical conditions of molecular clouds in other galaxies can be very difficult. For single dish observations, the beam size is usually larger than the angular diameter of typical molecular clouds, and so the line strengths are beam-diluted. Molecular clouds are known to be very clumpy (e.g. Stutzki & Güsten 1990), and so the average emission likely originates in a mixture of high and low density material. In addition, assumptions often have to be made about the optical depth of the emission lines. In the discussion below, we will initially assume that the  $^{12}\text{CO}$   $J=4-3$  and rarer [C I] emission are optically thin ( $\tau \ll 1$ ). In addition, we will concentrate on the larger peak located at  $(+5'', +5'')$  for which we have strong emission and good signal-to-noise ratios for all spectra including [C I].

### 4.1. Column Densities from Line Intensities

Atomic carbon emission is rather weak compared to CO emission (e.g. White et al. 1994; Israel et al. 1995) and is often thought to be optically thin. In the low optical depth limit, the column density is given by

$$N(\text{C}) = 1.9 \times 10^{15} (e^{E_1/kT_{\text{ex}}} + 3 + 5e^{(E_1-E_2)/kT_{\text{ex}}}) \int T_{\text{MB}} dv \quad (\text{cm}^{-2})$$

(Schilke et al. 1993; Phillips & Huggins 1981), where  $E_1/k$  is the energy of the  $J = 1$  level (23.6 K),  $E_2/k$  is the energy of the  $J=2$  level (62.5 K),  $T_{\text{ex}}$  is the excitation temperature of the gas, and  $\int T_{\text{MB}} dv$  is the integrated intensity of the [C I] line.

If we assume an excitation temperature of 24 K in M83 (Wall et al. 1993), the strength of the [C I] line at the (+5'',+5'') emission peak of 71.3 K km s<sup>-1</sup> ( $T_{\text{MB}}$ ) gives an atomic carbon column density of  $N(\text{C}) = 1 \times 10^{18}$  cm<sup>-2</sup>. (Adopting a higher excitation temperature of 50 K increases the column density by only 15%.) This column density is somewhat lower than that found in other starburst galaxies. For example, Israel et al. (1995) find atomic carbon column densities of  $7.7 \times 10^{18}$  cm<sup>-2</sup> in NGC 253 and White et al. (1994) find  $N(\text{C}) = 1.9 \times 10^{18}$  cm<sup>-2</sup> in the centre of M82. The larger column densities seen in both NGC 253 and M82 may be due to their nearly edge-on orientation ( $i = 78^\circ 5$  for NGC 253, Pence 1981;  $i = 80^\circ$  for M82, Shen & Lo 1995). If we correct the C I column densities to face-on values, we obtain  $N(\text{C}) = 9 \times 10^{17}$  cm<sup>-2</sup> for M83,  $1.5 \times 10^{18}$  cm<sup>-2</sup> for NGC 253, and  $3.3 \times 10^{17}$  cm<sup>-2</sup> for M82. This result suggests that C I column densities in M83 measured perpendicular to the disk may be comparable to those of other starburst galaxies.

Another way to correct for the differences in the geometry from one galaxy to another is to compare column density ratios of two different species, since both species are likely subject to the same geometry within a given galaxy. Such column density ratios need to be computed using beams of comparable size for both lines so that the filling factor of the emission is the same for each line. Since the <sup>12</sup>CO  $J=4-3$  and [C I] data have approximately the same beam size (12''), we will use them to calculate the ratio  $N(\text{C})/N(\text{CO})$ .

For the <sup>12</sup>CO  $J=4-3$  transition, the column density is given by

$$N(\text{CO}) = 4.3 \times 10^{14} \int T_{\text{MB}} dv \frac{\tau}{1 - e^{-\tau}} \quad (\text{cm}^{-2})$$

(White & Sandell 1995) where  $\tau$  is the optical depth of the <sup>12</sup>CO  $J=4-3$  emission and we assume  $T_{\text{ex}} = 23$  K. For optically thin gas, the strength of the CO  $J=4-3$  line in the emission peak at (+5'',+5'') indicates  $N(\text{CO}) = 1.5 \times 10^{17}$  cm<sup>-2</sup>. This column density is much lower than those previously found in other starburst galaxies (e.g.  $N(\text{CO}) = 5 \times 10^{18}$  cm<sup>-2</sup> for M82, Güsten et al. 1993;  $N(\text{CO}) \sim 3 \times 10^{19}$  cm<sup>-2</sup> for NGC 253, Israel et al. 1995). One possible explanation for this low CO column density is that our assumption that the gas is optically thin is incorrect. We would require an optical depth  $\tau \sim 30$  to obtain CO column densities similar to those in the starburst galaxy M82. Unfortunately, we do not have <sup>13</sup>CO  $J=4-3$  data with which to estimate the optical depth directly.

Another way to obtain the CO column density is by modeling the CO line ratios. The <sup>12</sup>CO  $J=4-3$  data were convolved to the same beam size as the <sup>12</sup>CO  $J=3-2$  data using the data reduction package COMB. The integrated intensity line ratios for the nucleus of M83 are shown in Figure 9. We estimate a total uncertainty in the line ratios of 30%. We used the line ratios for the emission peak at (+5'', +5'') to perform a Large Velocity Gradient (LVG) analysis. If

we adopt a kinetic temperature of 30 K,  $^{12}\text{CO } J=3-2/J=2-1 = 1.1$  (Wall et al. 1993),  $^{13}\text{CO } J=3-2/J=2-1 = 0.2$  (Wall et al. 1993),  $^{12}\text{CO } J=2-1/J=1-0 = 1$  (Wiklind et al. 1990), and  $^{12}\text{CO } J=4-3/J=3-2 = 1.13$  (Figure 9), we obtain a lower limit on the CO column density of  $N(\text{CO}) \gtrsim 3 \times 10^{18} \text{ cm}^{-2}$ . This value gives us a ratio of  $N(\text{C})/N(\text{CO}) < 0.33$ , which is similar to the value found for the starburst galaxy NGC 253 (Israel et al. 1995). We therefore adopt a  $N(\text{C})/N(\text{CO})$  ratio of  $0.33 \pm 0.10$  for M83. It should be noted that this ratio is only for the emission peak at  $(+5'', +5'')$ , while the values for NGC 253 and M82 are averaged over the nuclear region.

Since [C I] is thought to form in hot PDR regions associated with star formation, it is interesting to compare the  $N(\text{C})/N(\text{CO})$  ratios for these three galaxies to their star formation properties. By using the  $\text{H}\alpha$  surface brightness ( $\Sigma_{\text{H}\alpha}$  in  $\text{erg s}^{-1} \text{ pc}^{-2}$ ) divided by the gas surface density ( $\Sigma_{\text{H}}$  in  $\text{M}_{\odot} \text{ pc}^{-2}$ ) as an estimate of the star formation activity in the inner  $20''$  of each galaxy, Wall et al. (1993) find that M82 is the most active ( $\log(\Sigma_{\text{H}\alpha}/\Sigma_{\text{H}}) = 34.0$ ) followed by M83 ( $\log(\Sigma_{\text{H}\alpha}/\Sigma_{\text{H}}) = 33.3$ ) and NGC 253 ( $\log(\Sigma_{\text{H}\alpha}/\Sigma_{\text{H}}) = 31.8$ ). In this analysis, the  $\text{H}\alpha$  fluxes are not corrected for extinction and so may not be the best way to measure star formation activity. An alternate indicator of the strength of the starburst is the far-infrared luminosity, which indicates that M82 and NGC 253 are stronger starbursts ( $L_{\text{FIR}} = 3 \times 10^{10} L_{\odot}$  and  $1.5 \times 10^{10} L_{\odot}$  respectively) than M83 ( $L_{\text{FIR}} = 4 \times 10^9 L_{\odot}$ ) (Telesco & Harper 1980; Wall et al. 1993). Thus, in our small sample (see a summary in Table 1), there is no real indication that a strong starburst increases the  $N(\text{C})/N(\text{CO})$  ratio.

## 4.2. Integrated Intensity Line Ratios

The physical conditions in a molecular cloud or distant galaxy can be constrained using integrated intensity line ratios. By assuming the same regions in space are emitting the observed radiation, dividing the measured integrated intensities of two emission lines eliminates the unknown filling factor of the molecular gas in the beam, as long as the beam sizes are the same. Knowledge of how these line ratios vary in different conditions (such as cold dark clouds or hot star forming regions) as well as radiative transfer models allows determination of the conditions required to produce the observed line ratios.

The  $^{12}\text{CO } J=4-3/^{12}\text{CO } J=3-2$  integrated intensity line ratios vary substantially over the central region of M83 (Figure 9) with the highest ratios occurring towards the edges of the emission peaks. We would expect the  $^{12}\text{CO } J=4-3$  emission to be enhanced near the hotter regions of star formation in the centre of the galaxy. The  $^{12}\text{CO } J=4-3/J=3-2$  line ratio is highest to the right and left of the upper and lower peak of Figure 4, respectively, and a ridge of high ratios seems to run from the upper right to the lower left of Figure 9. This ridge corresponds with the arc of active star forming regions found by near infrared observations by Gallais et al. (1991; see also Figure 4 of Sofue & Wakamatsu 1994) as well as radio continuum observations by Turner & Ho (1994). We thus conclude that the peak  $^{12}\text{CO } J=4-3/J=3-2$  line ratios are likely excited



by the high temperatures associated with the arc of active star forming regions that encircles the nucleus of M83. Assuming local thermodynamic equilibrium (LTE), the high line ratios ( $>1$ ) indicate that the higher  $J$  transitions of CO are optically thin and are likely the result of the high temperatures and/or densities associated with star formation. In the LTE approximation, a  $^{12}\text{CO } J=4-3/J=3-2$  line ratio no greater than 1.7 is predicted for optically thin gas at an excitation temperature of 50 K, while the line ratio cannot exceed one if both transitions are optically thick. These data indicate that the  $^{12}\text{CO } J=4-3$  emission at  $(-5'', +5'')$  and  $(0'', -10'')$  from the nucleus of M83 is likely optically thin while the emission at  $(+5'', +5'')$  may be optically thick as suggested in the previous section.

Since the  $^{12}\text{CO } J=4-3$  and [C I] data have the same beam size, we are able to directly divide the observed integrated intensities to obtain line ratios. Ratios were only calculated for those regions where the integrated intensity is three times the rms noise. The results are shown in Figure 10. The [C I]/ $^{12}\text{CO } J=4-3$  integrated intensity line ratios are uniform at the  $2\sigma$  level and have an average value of  $0.25 \pm 0.03$ . This value is similar to that found in the starburst galaxy NGC 253 (0.27, Israel et al. 1995). In order to compare our value to the [C I]/ $^{12}\text{CO } J=1-0$  ratio, which is the most commonly published value, we must scale down our  $^{12}\text{CO } J=4-3$  data to equivalent  $^{12}\text{CO } J=1-0$  line strengths. We will again focus on the peak of the [C I] emission at  $(+5'', +5'')$ . Taking the [C I]/ $^{12}\text{CO } J=4-3$  line ratio of 0.21 (see Figure 10) and using the  $^{12}\text{CO } J=4-3/J=3-2$  line ratio of 1.02 (see Figure 9), the  $^{12}\text{CO } J=3-2/J=2-1$  ratio of 1.1 (Wall et al. 1993), and the  $^{12}\text{CO } J=2-1/J=1-0$  ratio of 1.0 (Wiklind et al. 1990) we obtain a [C I]/ $^{12}\text{CO } J=1-0$  ratio of 0.24 with an uncertainty of at least 30%. This ratio is higher than the value found in the starburst galaxy M82 (0.11, Schilke et al. 1993), the non-starburst spiral galaxy M33 (0.04-0.18, Wilson 1997), the starburst galaxy IC 342 (Büttegenbach et al. 1992), and our own Milky Way (0.16, Wright et al. 1991, assuming  $^{12}\text{CO } J=2-1/J=1-0 = 0.7$ , Sakamoto et al. 1994), but it is lower than that of the starburst galaxy NGC 253 (Israel et al. 1995). This comparison suggests that there is more C I being produced in M83 than in any of these other galaxies except NGC 253, but without accurate knowledge of the optical depth of the CO emission, this result is disputable.

While the actual value of the [C I]/CO line ratio may not yet tell us much about the conditions in the different regions of the galaxy, we can learn about the relative strengths of the processes creating and destroying C I and CO by comparing the [C I]/CO line ratio over different regions of the galaxy. If we can neglect optical depth effects, the [C I]/CO ratio is a measure of the relative quantities of the emitting material. It is interesting that the [C I]/ $^{12}\text{CO } J=4-3$  line ratio is uniform at the  $2\sigma$  level, while the  $^{12}\text{CO } J=4-3/J=3-2$  ratio varies substantially (up to  $\sim 50\sigma$ , see Figure 9). While we do not know exactly what conditions are required to produce high concentrations of C I, the uniformity of the [C I]/ $^{12}\text{CO } J=4-3$  line ratios likely indicates that the processes creating and destroying CO in the  $J = 4$  state and C I are comparable throughout the nucleus of M83. Line strengths are simultaneously dependent on temperature and optical depth, which suggests that the similarity in the [C I]/ $^{12}\text{CO } J=4-3$  line ratios can be explained

most simply by the emission originating in regions containing similar physical conditions. This interpretation suggests that the  $^{12}\text{CO } J=4-3$  emission may originate in the hot photodissociation regions surrounding massive stars that form inside the nuclear starburst of M83, since these are the regions that are likely to form atomic carbon.

## 5. Conclusions

This paper presents [C I],  $^{12}\text{CO } J=4-3$ , and  $^{12}\text{CO } J=3-2$  maps of the nucleus of the barred spiral galaxy M83 taken at the JCMT. The main results are summarized below.

1. We observe a double peaked structure in the molecular emission consistent with gas inflow along the bar collecting at the inner Lindblad resonance. The  $^{12}\text{CO } J=4-3$  emission suggests that some of the molecular gas has made it into the nucleus and is being heated by and possibly fueling the nuclear starburst. This result indicates that nuclear starbursts may occur even in galaxies which exhibit a double peaked emission structure, in contrast to the findings of Kenney et al. (1992).
2. We observe different morphologies in the  $^{12}\text{CO } J=4-3$  channel maps than in the  $^{12}\text{CO } J=3-2$  and  $^{12}\text{CO } J=1-0$  channel maps. These data suggest that  $^{12}\text{CO } J=1-0$  emission may not always be a good tracer of molecular gas in starburst galaxies, as the CO may be heated sufficiently to produce little emission in the  $J=1-0$  line. Thus, discretion should be applied in the interpretation of  $^{12}\text{CO } J=1-0$  emission as a tracer of molecular gas in starburst regions.
3. The observations also suggest that the double peaked emission may be the result of a molecular ring out of the plane of the galaxy oriented nearly perpendicular to the main disk. This torus of cooler gas would need to contain a disk of hotter gas that fills its central void in order to explain the observed morphology.
4. The [C I] line strength indicates carbon column densities of  $1 \times 10^{18} \text{ cm}^{-2}$  while CO emission indicates CO column densities of  $\sim 3 \times 10^{18} \text{ cm}^{-2}$  and  $\text{H}_2$  column densities of  $3 \times 10^{22} \text{ cm}^{-2}$  at the peak of the emission. The  $N(\text{C})/N(\text{CO})$  ratio at this location is  $0.33 \pm 0.10$  which is similar to those found in other starburst galaxies.
5. The twelve [C I]/ $^{12}\text{CO } J=4-3$  line ratios in the inner  $24'' \times 24''$  are uniform at the  $2\sigma$  level and have an average value of  $0.25 \pm 0.03$ , similar to those of other starburst galaxies. The uniformity of the line ratios suggests that both the high-excitation CO emission and atomic carbon form in photodissociation regions in the starburst nucleus.
6. The  $^{12}\text{CO } J=4-3/^{12}\text{CO } J=3-2$  integrated intensity line ratios vary substantially over the central region of M83 with the highest ratios occurring towards the edges of the emission peaks. The  $^{12}\text{CO } J=4-3/J=3-2$  line ratios seem to be enhanced along an arc of active star

forming regions. The high line ratios ( $>1$ ) indicate that the higher  $J$  transitions of CO are optically thin and are likely the result of the high temperatures and/or densities associated with star formation.

The JCMT is operated by the Royal Observatories on behalf of the Particle Physics and Astronomy Research Council of the United Kingdom, the Netherlands Organization for Scientific Research, and the National Research Council of Canada. This research has been supported by a research grant to C. D. W. from NSERC (Canada).

## REFERENCES

- Anantharamaiah, K. R., & Goss, W. M., 1996, *ApJ*, 466, L13
- Balcells, M., & Quinn, P. J., 1990, *ApJ*, 361, 381
- Bohlin, R. C., Cornett, R. H., Hill, J. K., Smith, A. M., & Stecher, T. P., 1983, *ApJ*, 274, L53
- Boisse, P., 1990, *A&A*, 228, 483
- Büttgenbach, T. H., Keene, J., Phillips, T. G., & Walker, C. K., 1992, *ApJ*, 397, L15
- Combes, F., 1988, in *Galactic and Extragalactic Star Formation*, ed. R. E. Pudritz & M. Fich (Dordrecht: Kluwer), 475
- Comte, G., 1981, *A&AS*, 44, 441
- Cowen, J. J., & Branch, D., 1985, *ApJ*, 293, 400
- Gallais, P., Rouan, D., Lacombe, F., Tiphene, D., & Vauglin, I., 1991, *A&A*, 243, 309
- Güsten, R., Serabyn, E., Kasemann, C., Schinckel, A., Schneider, G., Schultz, A., & Young, K., 1993, *ApJ*, 402, 537
- Handa, T., Nakai, N., Sofue, Y., Hayashi, M., & Fujimoto, M., 1990, *PASJ*, 42, 1
- Handa, T., Ishizuki, S., & Kawabe, R., 1994, in *Astronomy with Millimeter and Submillimeter Wave Interferometry*, IAU Colloquium No. 140, ed. M. Ishiguro & W. J. Welch, 341
- Hernquist, L., & Mihos, J. C., 1995, *ApJ*, 448, 41
- Ishizuki, S., Kawabe, R., Ishiguro, M., Okumura, S. K., Morita, K.-I., Chikada, Y., & Kasuga, T., 1990, *Nature*, 344, 224
- Israel, F. P., White, G. J., & Baas, F., 1995, *A&A*, 302, 343
- Keene, J., Blake, G. A., Phillips, T. G., Huggins, P. J., & Beichman, C. A., 1985, *ApJ*, 299, 967
- Kenney, J. D. P., Wilson, C. D., Scoville, N. Z., Devereux, N. A., & Young, J. S., 1992, *ApJ*, 395, L79

- Larkin, J. E., Graham, J. R., Matthews, K., Soifer, B. T., Beckwith, S., Herbst, T. M., & Quillen, A. C., 1994, *ApJ*, 420, 159
- Leung, C. M., Herbst, E., & Huebner, W. F., 1984, *ApJS*, 56, 231
- Mihos, J. C., & Hernquist, L., 1994, *ApJ*, 425, L13
- Morton, D. C., Drake, J. F., Jenkins, E. B., Rogerson, J. B., Spitzer, L., & York, D. G., 1973, *ApJ*, 181, L103
- Pence, W. D., 1981, *ApJ*, 247, 473
- Phillips, T. G., & Huggins, P. J., 1981, *ApJ*, 251, 533
- Plume, R., Jaffe, D. T., & Keene, J., 1994, *ApJ*, 425, L49
- Quinn, P. J., Hernquist, L., & Fullager, D., 1993, *ApJ*, 403, 74
- Rogstad, D. H., Lockhart, I. A., & Wright, M. C. H., 1974, *ApJ*, 193, 309
- Sakamoto, S., Hayashi, M., Hasegawa, T., Handa, T., & Oka, T., 1994, *ApJ*, 425, 641
- Schilke, P., Carlstrom, J. E., Keene, J., & Phillips, T. G., 1993, *ApJ*, 417, L67
- Shen, J., & Lo, K. Y., 1995, *ApJ*, 445, L99
- Shlosman, I., Frank, J., & Begelman, M. C., 1989, *Nature*, 338, 45
- Sofue, Y., & Wakamatsu, K. -I., 1994, *AJ*, 107, 1018
- Sørensen, S. -A., Matsuda, T., & Fujimoto, M., 1976, *Ap&SS*, 43, 491
- Stutzki, J., & Güsten, R., 1990, *ApJ*, 356, 513
- Talbot, R. J., Jr., Jensen, E. B., & Dufour, R. J., 1979, *ApJ*, 229, 91
- Telesco, C. M., & Harper, D. A., 1980, *ApJ*, 235, 392
- Tilanus, R. P. J., Tacconi, L. J., Sutton, E. C., Zhou, S., Sanders, D. B., Wynn-Williams, C. G., Lo, K. Y., & Stephens, S. A., 1991, *ApJ*, 376, 500
- Tully, R. B., 1988, *Nearby Galaxies Catalogue*, (Cambridge: Cambridge Press)
- Turner, J. L., & Ho, P. T. P., 1994, *ApJ*, 421, 122
- Wall, W. F., Jaffe, D. T., Bash, F. N., Israel, F. P., Maloney, P. R., & Baas, F., 1993, *ApJ*, 414, 98
- White, G. J., Ellison, B., Claude, S., Dent, W. R. F., & Matheson, D. N., 1994, *A&A*, 284, L23
- White, G. J., & Sandell, G., 1995, *A&A*, 299, 179
- Wiklind, T., Rydbeck, G., Hjalmarsen, Å., & Bergman, P., 1990, *A&A*, 232, L11
- Wilson, C. D., 1997, *ApJ*, 487, L49
- Wright, E. L., et al., 1991, *ApJ*, 381, 200

Fig. 1.— Individual  $^{12}\text{CO } J=3-2$  spectra for the centre of the galaxy M83. The orientation is such that north corresponds to an angle  $135^\circ$  from the positive  $x$ -axis and the bar runs along the  $x$ -axis. The temperature scale is main beam temperature ( $T_{\text{MB}}$ ). The map is centred at  $\alpha = 13^{\text{h}}34^{\text{m}}11^{\text{s}}.53$ ,  $\delta = -29^\circ36'42''.20$  (B1950.0). The velocity range plotted is  $300 \text{ km s}^{-1}$  to  $700 \text{ km s}^{-1}$  at a resolution of  $16.2 \text{ km s}^{-1}$  (18.75 MHz) and the vertical range is  $-0.5 \text{ K}$  to  $3.0 \text{ K}$ .

Fig. 2.— Individual  $^{12}\text{CO } J=4-3$  spectra for M83. The temperature scale is main beam temperature ( $T_{\text{MB}}$ ). The map centre and orientation is the same as Figure 1. The velocity range plotted is  $200 \text{ km s}^{-1}$  to  $800 \text{ km s}^{-1}$  at a resolution of  $12.2 \text{ km s}^{-1}$  (18.75 MHz) and the vertical range is from  $-0.5 \text{ K}$  to  $5.0 \text{ K}$ .

Fig. 3.— Individual [C I] spectra for M83. The temperature scale is main beam temperature ( $T_{\text{MB}}$ ). The map centre and orientation is the same as Figure 1. The velocity range plotted is  $200 \text{ km s}^{-1}$  to  $800 \text{ km s}^{-1}$  at a resolution of  $15.1 \text{ km s}^{-1}$  (25 MHz) and the vertical range is  $-0.5 \text{ K}$  to  $1.0 \text{ K}$ .

Fig. 4.— Integrated intensity map for the  $^{12}\text{CO } J=3-2$  transition in M83. The emission is integrated from  $400 \text{ km s}^{-1}$  to  $600 \text{ km s}^{-1}$  and is given in  $\text{K km s}^{-1}$  ( $T_{\text{MB}}$ ). The contour interval is  $25 \text{ K km s}^{-1}$  with the lowest contour being  $-25 \text{ K km s}^{-1}$ . The maximum value is  $290 \text{ K km s}^{-1}$ . The emission shows a double peaked structure that is consistent with gas inflow along the bar collecting at the ILR, or possibly an inclined ring of molecular gas.

Fig. 5.— Integrated intensity map for the  $^{12}\text{CO } J=4-3$  transition in M83. The emission is integrated from  $400 \text{ km s}^{-1}$  to  $600 \text{ km s}^{-1}$  and is given in  $\text{K km s}^{-1}$  ( $T_{\text{MB}}$ ). The contour interval is  $25 \text{ K km s}^{-1}$  with the lowest contour being  $-25 \text{ K km s}^{-1}$ . The maximum value is  $357 \text{ K km s}^{-1}$ . These data also show the same double peaked structure as the  $^{12}\text{CO } J=3-2$  data.

Fig. 6.— Integrated intensity map for the [C I] transition in M83. The emission is integrated from  $400 \text{ km s}^{-1}$  to  $600 \text{ km s}^{-1}$  and is given in  $\text{K km s}^{-1}$  ( $T_{\text{MB}}$ ). The contour interval is  $5.0 \text{ K km s}^{-1}$  with the lowest contour being  $-5.0 \text{ K km s}^{-1}$ . The maximum value is  $78 \text{ K}$ . These data show a similar ‘elbow’ structure as the  $^{12}\text{CO } J=4-3$  data. The peaks overlap (within pointing uncertainties) the two peaks and bend in the  $^{12}\text{CO } J=4-3$  data.

Fig. 7.— Integrated intensity channel maps for the  $^{12}\text{CO } J=3-2$  transition in M83. The integrated emission is given in  $\text{K km s}^{-1}$  ( $T_{\text{MB}}$ ). The velocity interval is  $10 \text{ km s}^{-1}$  with the first panel centred at  $440 \text{ km s}^{-1}$ . Contours levels are shown at  $2.5 \text{ K km s}^{-1}$  intervals with the lowest contour at  $-7.5 \text{ K km s}^{-1}$ . In this figure we can see the emission to the north peak at velocities lower than the emission to the south.

Fig. 8.— Integrated intensity channel maps for the  $^{12}\text{CO } J=4-3$  transition in M83. The integrated emission is given in  $\text{K km s}^{-1}$  ( $T_{\text{MB}}$ ). The velocity interval is  $10 \text{ km s}^{-1}$  with the first panel centred at  $440 \text{ km s}^{-1}$ . Contours levels are shown at  $5.0 \text{ K km s}^{-1}$  intervals with the lowest contour at  $-5.0 \text{ K km s}^{-1}$ . In this figure we can see the emission peak shift to the south due to the rotation

of the molecular gas. Note how it peaks at the centre near velocities of  $\sim 520$  km s $^{-1}$ , in contrast to the  $^{12}\text{CO } J=3-2$  data.

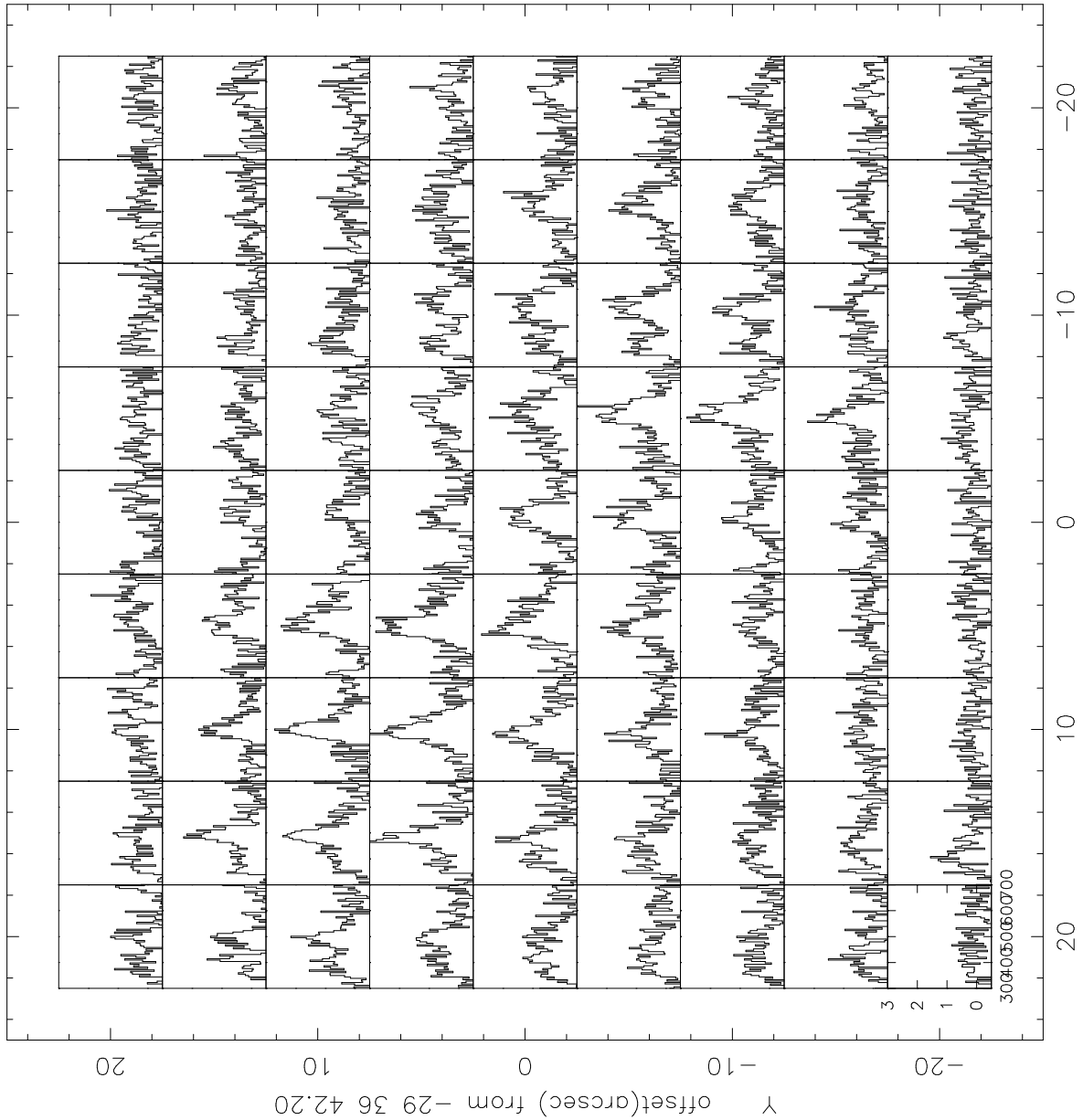
Fig. 9.— Integrated intensity line ratios for  $^{12}\text{CO } J=4-3/^{12}\text{CO } J=3-2$  at 22 locations in M83. The  $^{12}\text{CO } J=4-3$  data has been convolved to the same beam size as the  $^{12}\text{CO } J=3-2$  data. The line ratio peaks in a rough line that runs from the upper right to the lower left corner of the diagram. This strip corresponds to a ring of active star forming regions.

Fig. 10.— Integrated intensity ( $T_{\text{MB}}$ ) line ratios for  $[\text{C I}]/^{12}\text{CO } J=4-3$  at 12 locations in M83. Only those locations where the signal to noise in the  $[\text{C I}]$  and  $^{12}\text{CO } J=4-3$  integrated intensity was greater than three are shown. The data were taken with comparable beam sizes at the JCMT. The line ratios are uniform at the  $2\sigma$  level, which indicates that similar processes are responsible for C I and  $^{12}\text{CO } J=4-3$  emission from the nucleus of M83.

Table 1. Properties of Starburst Galaxies

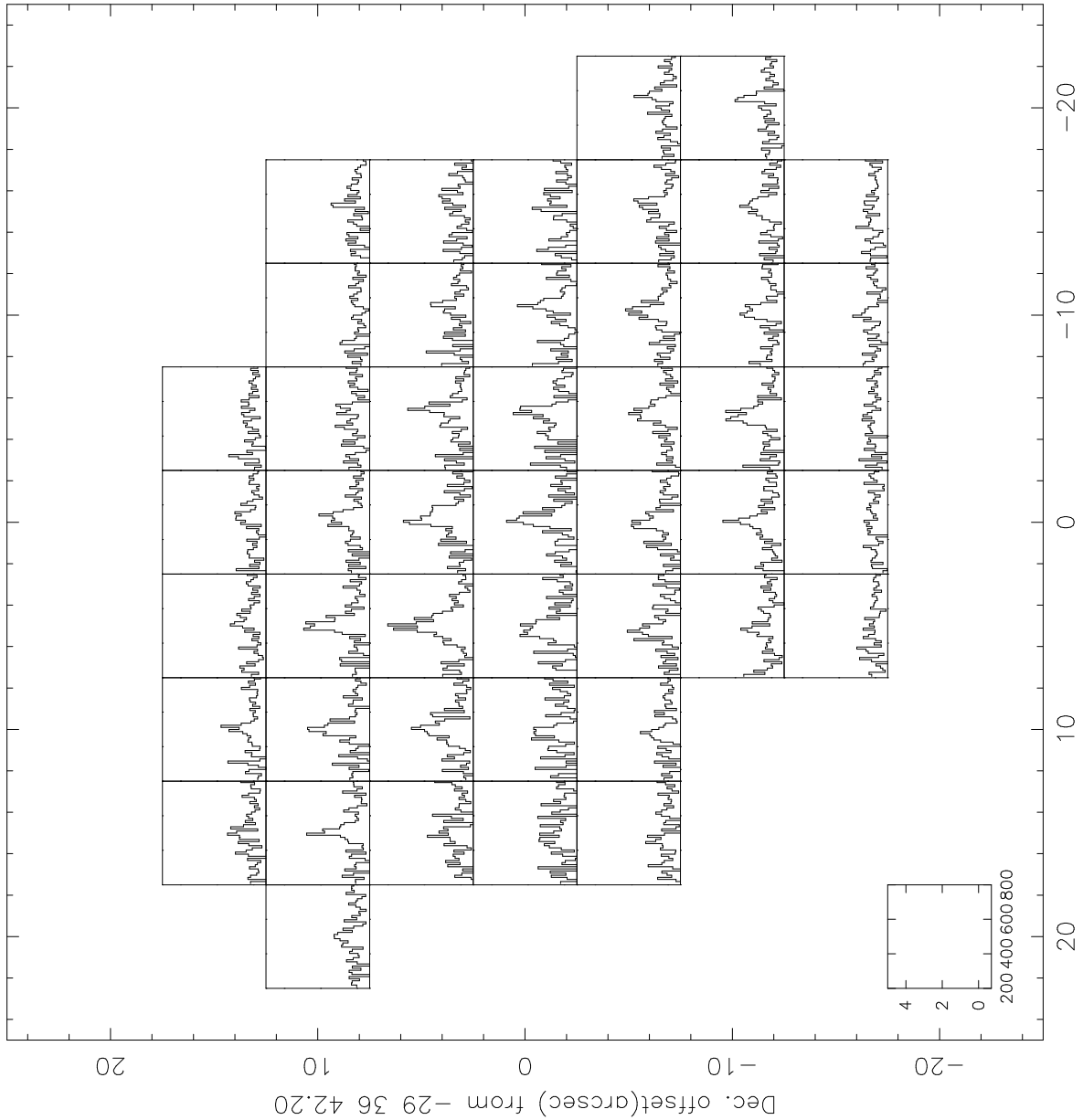
Galaxy	$i$	$N(\text{C})$ ( $\text{cm}^{-2}$ )	$N(\text{CO})$ ( $\text{cm}^{-2}$ )	$\frac{N(\text{C})}{N(\text{CO})}$	$L_{\text{FIR}}$ ( $L_{\odot}$ )	$\log(\Sigma \text{H}\alpha / \Sigma \text{H})$ $\log\left(\frac{\text{erg s}^{-1} \text{pc}^{-2}}{M_{\odot} \text{pc}^{-2}}\right)$	References
M83	$24^{\circ}$	$1 \times 10^{18}$	$> 3 \times 10^{18}$	$0.33 \pm 0.10$	$4 \times 10^9$	33.3	1, 2, 3
M82	$80^{\circ}$	$1.9 \times 10^{18}$	$5 \times 10^{18}$	0.5	$3 \times 10^{10}$	34.0	2, 3, 4, 5, 6
NGC 253	$78^{\circ}5$	$7.7 \times 10^{18}$	$3 \times 10^{19}$	0.2 – 0.3	$1.5 \times 10^{10}$	31.8	2, 3, 7, 8

(1) Comte 1981. (2) Telesco & Harper 1980. (3) Wall et al. 1993. (4) Shen & Lo 1995. (5) White et al. 1994. (6) Güsten et al. 1993. (7) Pence 1981. (8) Israel et al. 1995.

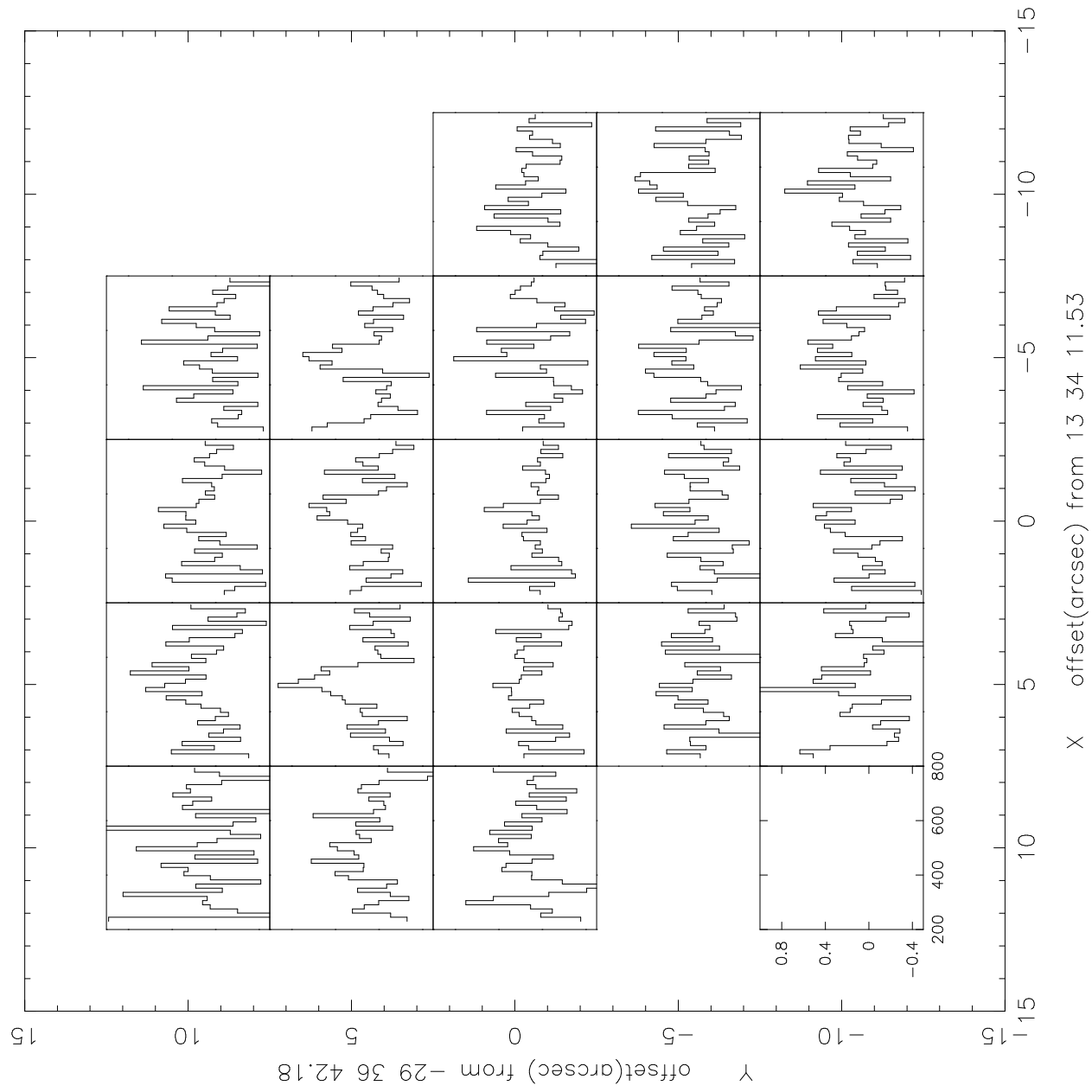


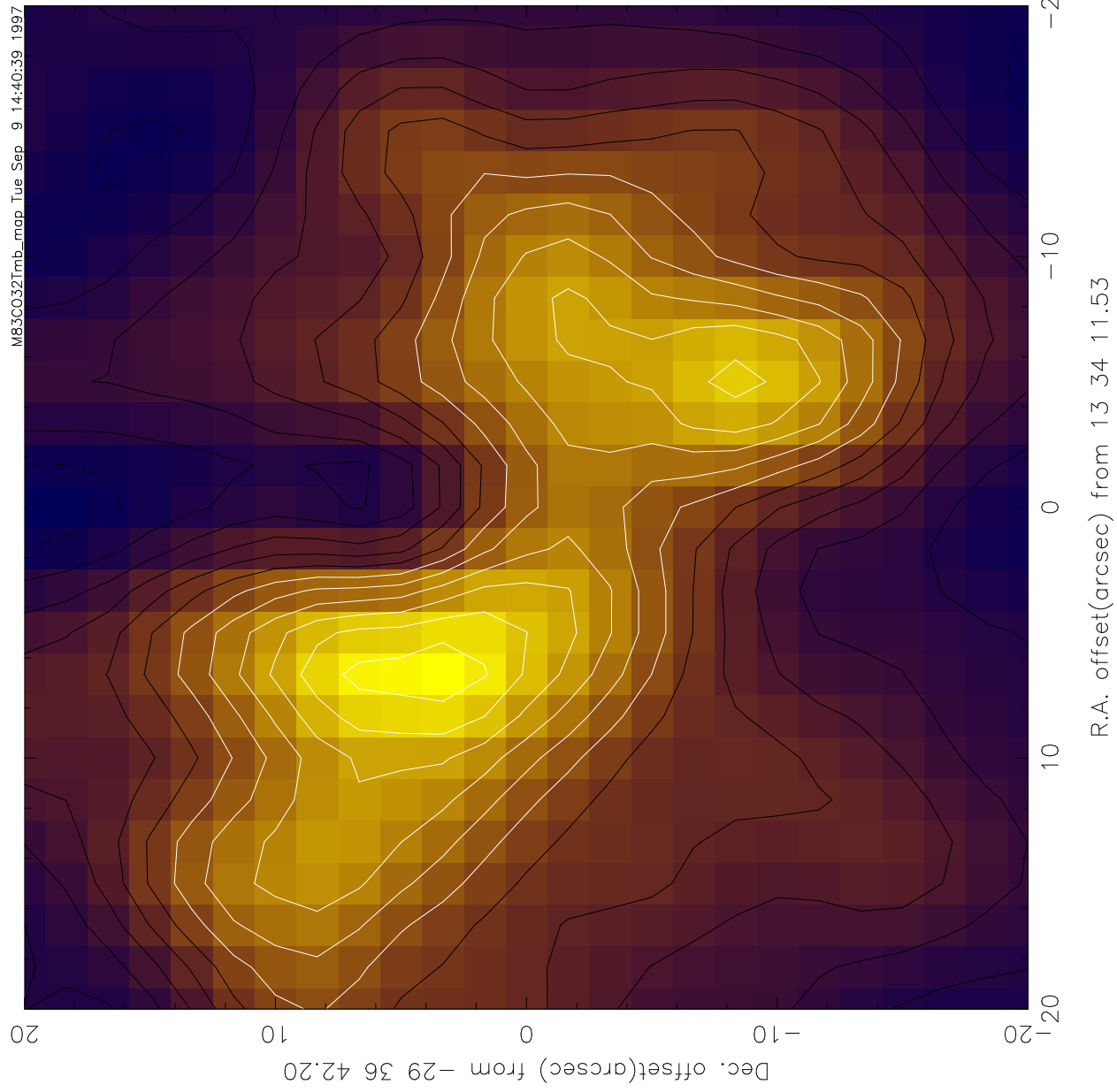
X offset(arcsec) from 13 34 11.53

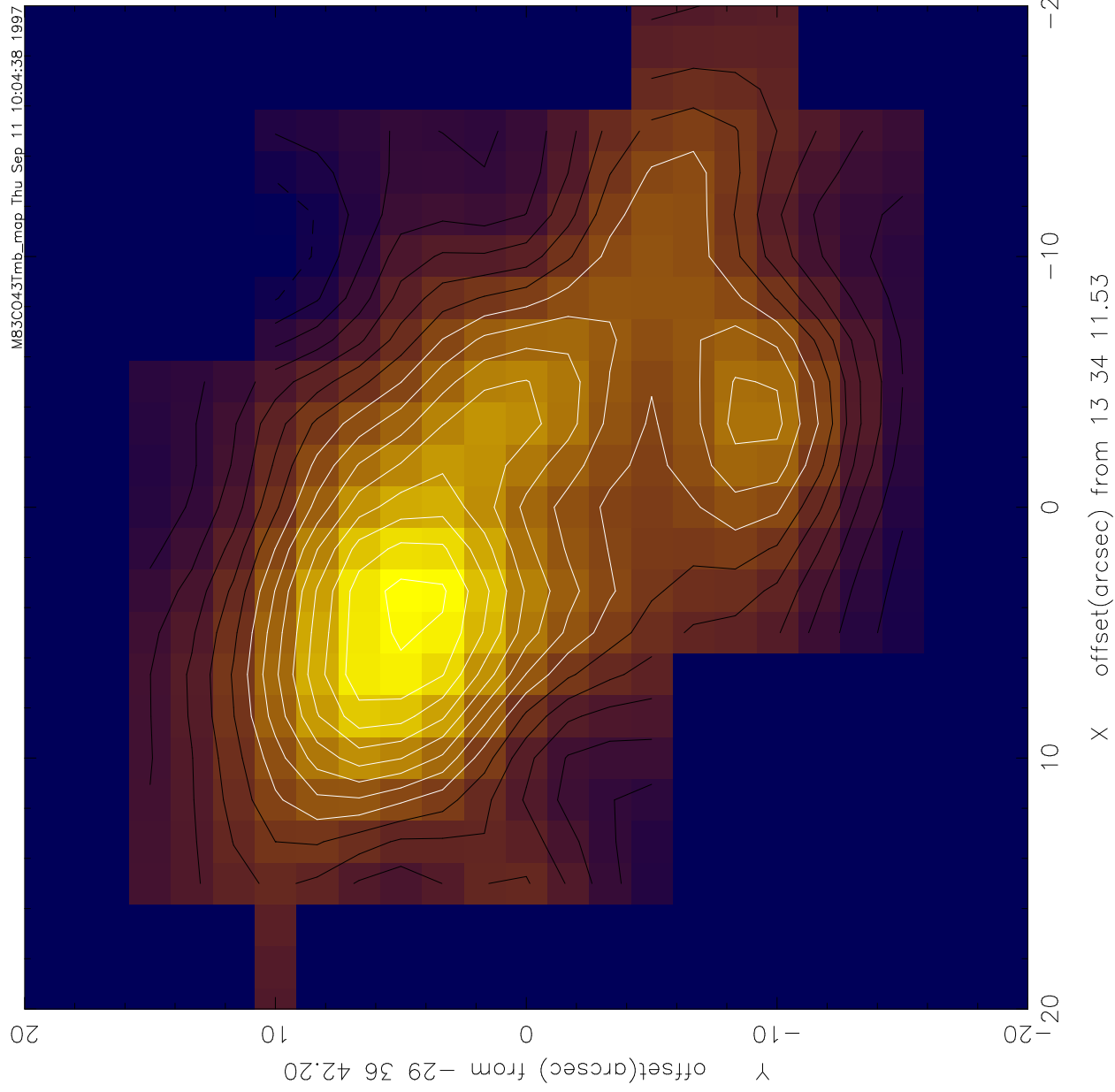


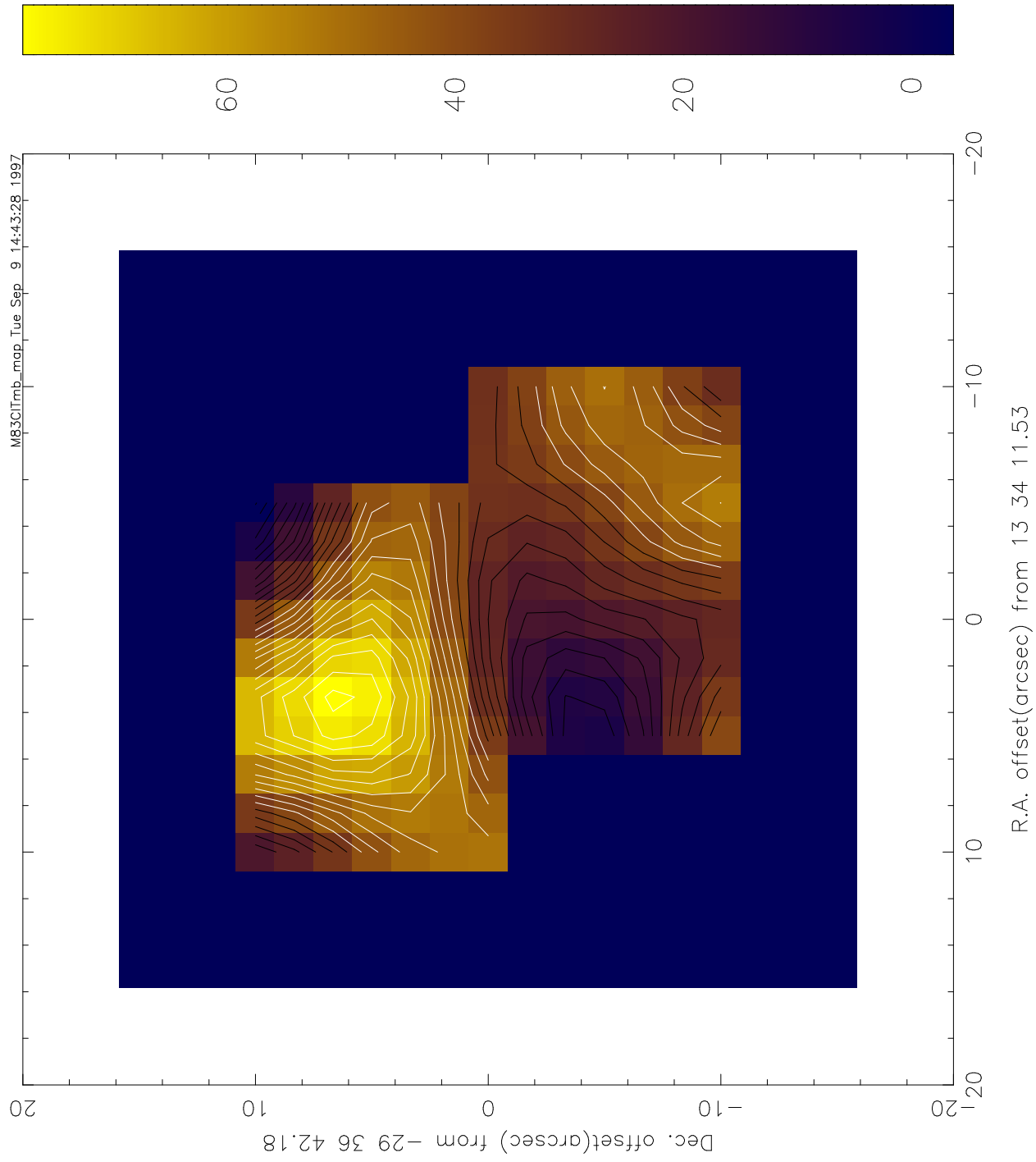


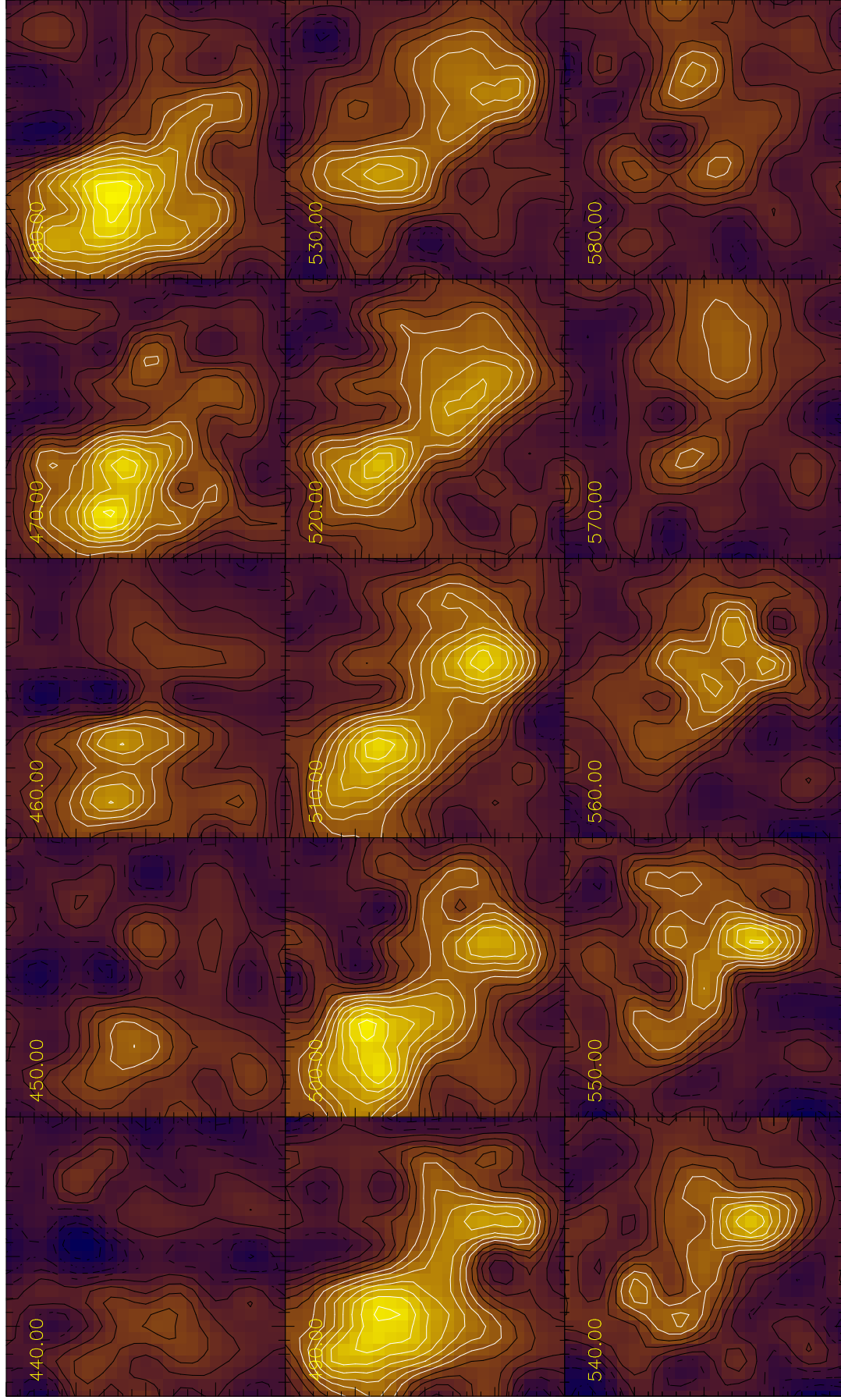
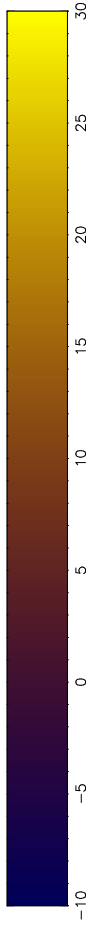
R.A. offset(arcsec) from 13 34 11.53



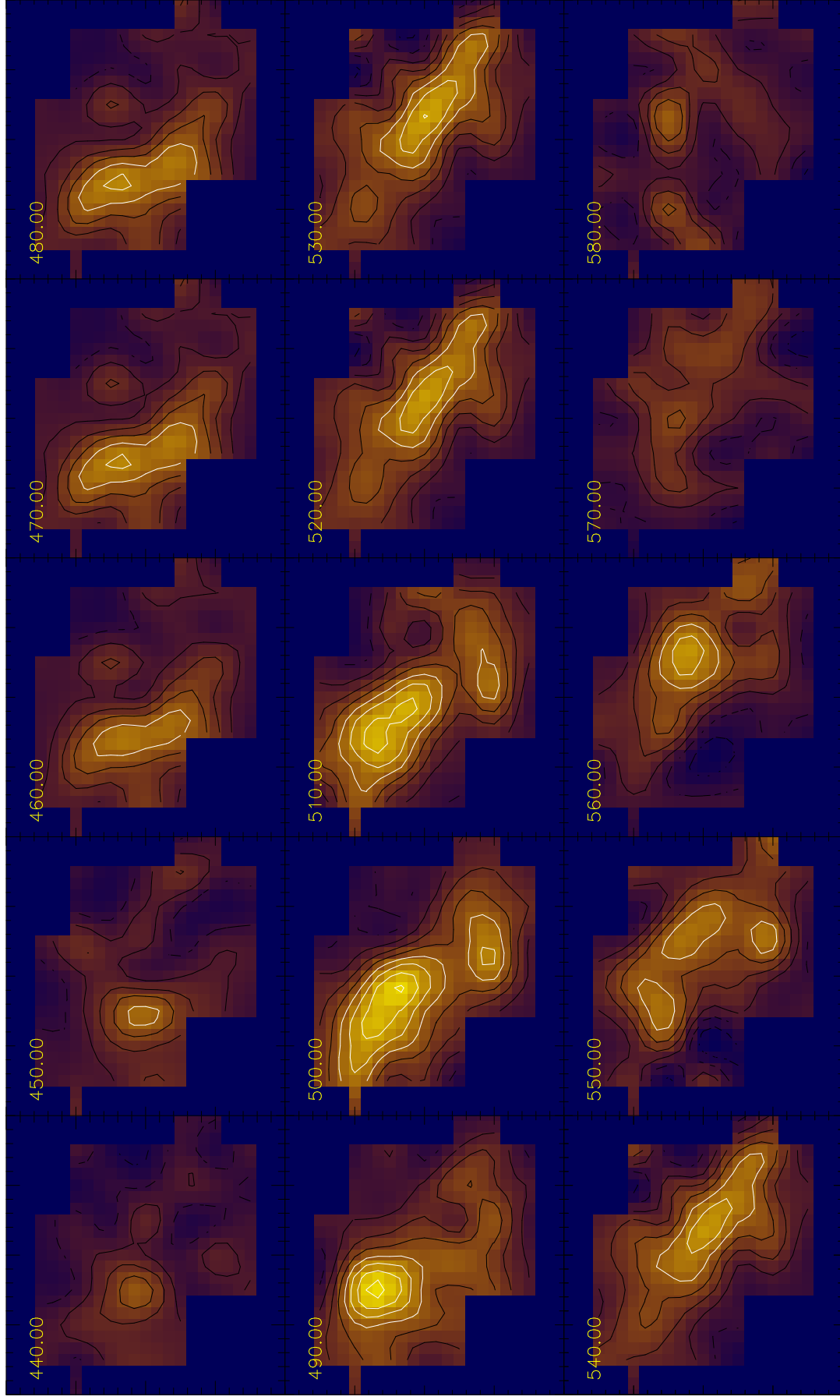
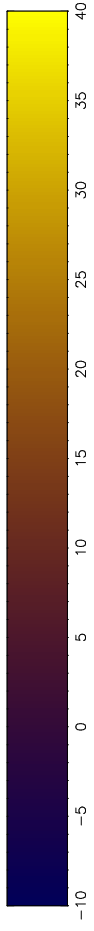








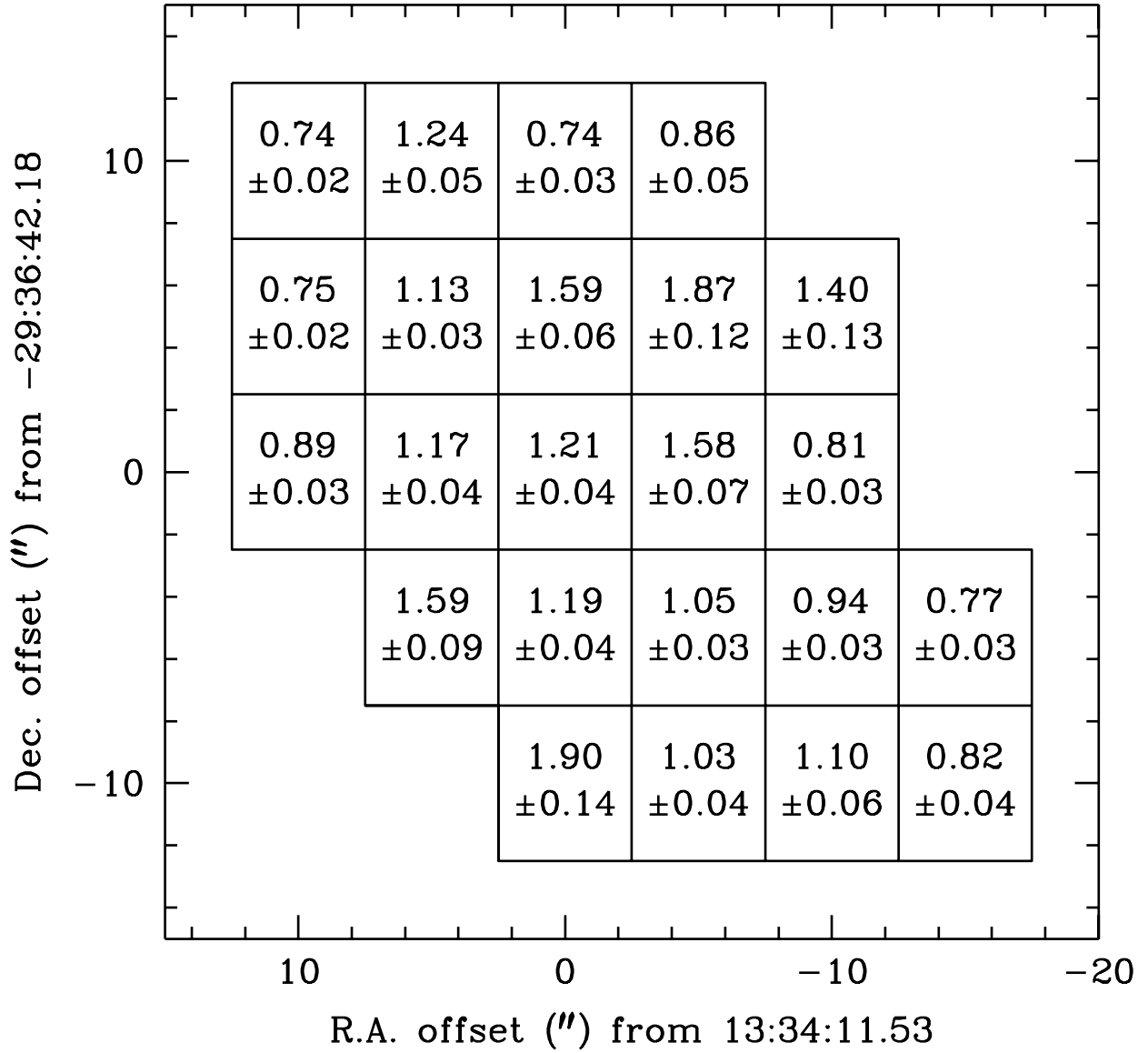
Dec. offset(arcsec) from -29 36 42.20  
R.A. offset(arcsec) from 13 34 11.53



Dec. offset(arcsec) from -29 36 42.20  
120 10 0 -10 -20

R.A. offset(arcsec) from 13 34 11.53

$^{12}\text{CO } J=4-3/J=3-2$





[CI]/<sup>12</sup>CO J=4-3

